Biosensors and Bioelectronics 133 (2019) 39–47

Contents lists available at ScienceDirect

Biosensors and Bioelectronics

journal homepage: www.elsevier.com/locate/bios

Design of a multi-sensor platform for integrating extracellular acidification rate with multi-metabolite flux measurement for small biological samples

Yusra M. Obeidat[a,b], Ming-Hao Cheng[a], Giovana Catandi[c], Elaine Carnevale[c], Adam J. Chicco[c,d], Thomas W. Chen[a,d,*]

[a] Department of Electrical and Computer Engineering, Colorado State University, Fort Collins, CO 80523, USA
[b] Electronic Engineering Department, Hijjawi Faculty for Engineering Technology, Yarmouk University, Irbid P.O. Box 21163, Jordan
[c] Department of Biomedical Sciences, Colorado State University, Fort Collins, CO 80523, USA
[d] School of Biomedical Engineering, Colorado State University, Fort Collins, CO 80523, USA

ARTICLE INFO

Keywords:
Acidification rate
Sensor
Clark oxygen
Equine embryo
Multi-sensors
Glucose
Lactate
Interference

ABSTRACT

Rates of cellular oxygen consumption (OCR) and extracellular acidification (ECAR) are widely used proxies for mitochondrial oxidative phosphorylation (OXPHOS) and glycolytic rate in cell metabolism studies. However, ECAR can result from both oxidative metabolism (carbonic acid formation) and glycolysis (lactate release), potentially leading to erroneous conclusions about metabolic substrate utilization. Co-measurement of extracellular glucose and lactate flux along with OCR and ECAR can improve the accuracy and provide better insight into cellular metabolic processes but is currently not feasible with any commercially available instrumentation. Herein, we present a miniaturized multi-sensor platform capable of real-time monitoring of OCR and ECAR along with extracellular lactate and glucose flux for small biological samples such as single equine embryos. This multiplexed approach enables validation of ECAR resulting from OXPHOS versus glycolysis, and expression of metabolic flux ratios that provide further insight into cellular substrate utilization. We demonstrate expected shifts in embryo metabolism during development and in response to OXPHOS inhibition as a model system for monitoring metabolic plasticity in very small biological samples. Furthermore, we also present a preliminary interference analysis of the multi-sensor platform to allow better understanding of sensor interference in the proposed multi-sensor platform. The capability of the platform is illustrated with measurements of multi-metabolites of single-cell equine embryos for assisted reproduction technologies. However, this platform has a wide potential utility for analyzing small biological samples such as single cells and tumor biopsies for immunology and cancer research applications.

1. Introduction

Cellular adenosine triphosphate (ATP) is produced by aerobic and anaerobic pathways. Energy metabolism varies in cells based on their nature, activity, and microenvironment. Abnormal cellular bioenergetics are likely associated with diseases such as obesity, diabetes, cancer, neurodegeneration and cardiomyopathy (Watanabe et al., 2006; Sridharan et al., 2007). Phenotypic changes are driven by underlying adjustments of cellular bioenergetics which often have unique profiles (Butler, 2005; Nicholls et al., 2007; Lambert and Brand, 2007).

Measurements of cellular respiration in terms of oxygen consumption rate (OCR) and extracellular acidification (ECAR) are the most common techniques employed to study cellular energy metabolism and have contributed significantly to our present understanding of bioenergetics in health and disease (Nicholls et al., 2007). By monitoring changes in dissolved oxygen (DO) and pH in the media surrounding cells over time, the rates of mitochondrial respiration and glycolytic metabolism can be estimated, respectively (Owicki and Parce, 1992). However, OCR does not provide direct information about cellular substrate utilization, and ECAR can result from both glycolysis (cellular lactate/proton symport) and oxidative metabolism (carbonic acid formation in media), leading to potentially misleading results (Mookerjee and Brand, 2015). Co-measurement of extracellular glucose and lactate flux along with OCR and ECAR can resolve these concerns and provide further insight into cellular metabolic processes but is currently not feasible with any commercially available instrumentation. Fluorescence

* Corresponding author at: Department of Electrical & Computer Engineering, School of Biomedical Engineering, Colorado State University, Fort Collins, CO 80523, USA.
E-mail address: thomas.chen@colostate.edu (T.W. Chen).

https://doi.org/10.1016/j.bios.2019.02.069
Received 5 December 2018; Received in revised form 25 February 2019; Accepted 26 February 2019
Available online 11 March 2019
0956-5663/ Published by Elsevier B.V.

analysis is widely used for many applications, providing non-invasive, easily operated, disposable, and low-cost assays (Wang and Wolfbeis, 2014; Bavli et al., 2016). Several studies have used the optical techniques to measure pH (Wu et al., 2018; Mousavi et al., 2016), oxygen (Bavli et al., 2016; Wu et al., 2018), glucose (Bennett et al., 1996), and lactate (Pilatus et al., 2001). Agilent's Extracellular Flux Analyzer is another example of using the optical method for measuring cell respiration and ECAR in cell cultures (TeSlaa and Teitell, 2014; Mookerjee and Brand, 2015). However, in addition to its high cost, it was designed to analyze respiration and ECAR separately in a small volume of seeded cells, rather than simultaneously in single cells. There is increasing interest in monitoring metabolic flux in single cells and very small biological samples for immunology and cancer research (Vasdekis and Stephanopoulos, 2015), and assisted reproduction applications (Scott et al., 2018), providing an impetus for new technological innovation in these areas.

Electrochemical sensors allow miniaturization and higher degree of integration of multiple sensors in a tiny volume for real-time measurements of multiple analytes in diverse biological systems, such as single cells (Wang et al., 2012) to micro-samples from patients in a clinical setting (Feuerstein et al., 2010). Additionally, electrochemical sensors can enable label-free, real-time intracellular and extracellular measurements without perturbing the system under investigation (Wang et al., 2012). There have been a number of reported studies that used electrochemical methods for measuring DO (Obeidat and Chen, 2016; Obeidat et al., 2018a), glucose (Pemberton et al., 2009; Obeidat et al., 2018b), lactate (Rawson et al., 2009; Obeidat et al., 2018b), and pH (McConnell et al., 1992; Liao et al., 1998).

Various approaches have been proposed to facilitate integration of electrochemical sensors for real-time monitoring of multiple analytes (Eklund et al., 2004; Pemberton et al., 2014). Some of them combine amperometric and potentiometric sensors to measure changes to cellular bioenergetics in real-time (Eklund et al., 2004). However, these existing multi-sensor methods have mainly focused on individual sensor performance (sensitivity and selectivity, etc.), and lack an overall system-level approach needed for sensor integration. Specifically, the existing methods lack the attention and discussions on potential interference between sensors residing in close proximity within a microchamber and relying on the same intermediate analytes (H_2O_2 in this case for both the glucose and lactate sensors).

This paper presents a multi-sensor platform to measure DO, glucose, lactate, and pH in real-time for small biological samples. Previously, we have reported a similar platform to characterize DO, glucose and lactate flux in bovine embryo (Obeidat et al., 2018b). In the work described herein, pH sensor was added to the platform to measure ECAR. We demonstrate 1) the relationships among DO and glucose consumption rate (GCR), lactate production rate (LPR), and ECAR during equine embryo development; 2) the effect of blocking OXPHOS with oligomycin (forcing cells to rely on glycolysis), on corresponding changes in all four analytes during and after the switch; and 3) the value of generating metabolite flux ratios to validate ECAR measurements and compliment the results from individual sensors, thus providing additional insight to cellular metabolic plasticity under these conditions.

In addition to sensor performance, preliminary results on sensor interference under a scenario of tightly coupled multiple sensor configuration for glucose and lactate is also provided. We would like to stress the preliminary nature of the interference data presented in this paper. It is not our intent to provide comprehensive discussions of this important topic for multi-sensor systems. But rather to provide a foundation for further studies and discussions.

2. Materials and methods

2.1. Materials and reagents

SU8-2050 and SU8 developer were purchased from MicroChem Corp (MA, USA). Megaposit MF −26A developer and S1813 photoresist were purchased from Capitol Scientific, Inc (Austin, TX). Indium Tin Oxide (ITO) coated glass substrates, 5% w/w Nafion perfluorinated resin, glucose oxidase (GOx), lactate oxidase (LOx), D- (+)-glucose, sodium L-lactate, phosphate buffer saline (PBS), Tween-20, oligomycin, FCCP, and bovine serum albumin (BSA) were purchased from Sigma Aldrich (St. Louis, Missouri). Sodium sulfite (Na_2SO_3) was purchased from Eisen-Golden laboratories (Berkeley, California). G-MOPS™ medium (respiration buffer) and paraffin oil (OVOIL™) were purchased from Vitrolife (Denver, Colorado). pH meter was purchased from (Hanna instruments, Woonsocket RI, USA). Oakton DO6+ DO meter (Cole-Parmer, Vernon Hills, Illinois).

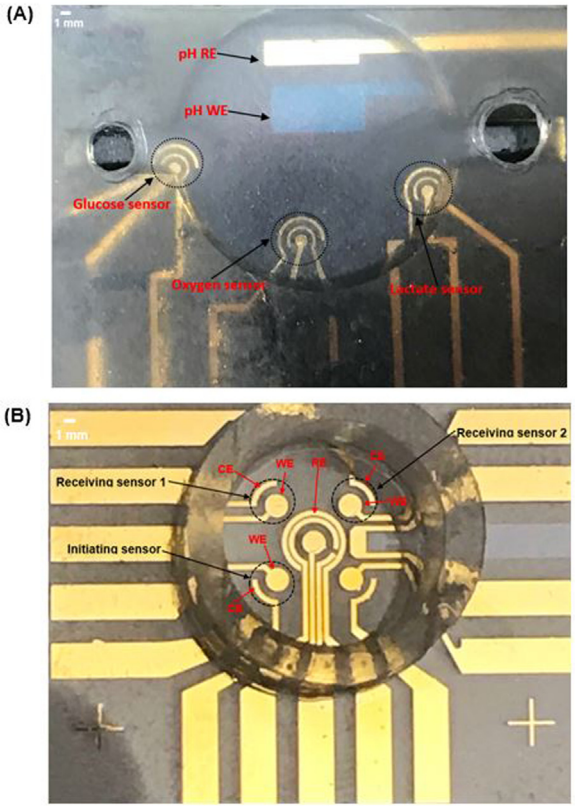

Fig. 1. (A) Complete design covered by a glass lid. **(B)** The sensor design used for interference test.

2.2. Electrodes and chamber designs and manufacturing

The multi-sensor platform had an ITO electrode for pH measurement and gold (Au) electrodes for measuring other metabolites. Using the combination of photolithography, thermal evaporation, and lift-off, the 24.5 mm × 24.5 mm sensor chip is shown in Fig. 1**A**. Details of the mask design, photolithography, etching, metal evaporation, and lift-off are included in S.1 in Supplementary material. A 12-mm diameter and 3-mm deep micro-chamber containing all sensors was made using SU8 with details provided in S.1.4 in Supplementary material.

2.3. Sensors surfaces modification

Techniques for surface modifications for oxygen, glucose and lactate sensors were the same as described in our previous paper (Obeidat et al., 2018b) and as added to S.2 in Supplementary material.

2.4. Sensor activation voltages

Activation voltages for DO, glucose, and lactate, were found to be

-0.6 V, 0.4 V, and 0.4 V, respectively. Details of the experiments to determine the activation voltages and the results are in S.3 in Supplementary material.

2.5. Sensors calibration

2.5.1. Calibration for oxygen, glucose and lactate sensors

The initial calibration curves as described previously (Obeidat et al., 2018b) with details are included in S.7 in Supplementary material. We assumed a fixed pH value of the buffer at the beginning of experiments. However, during cell basal respiration and glycolysis, the pH level decreases which, in turn, affects the response of both glucose and lactate enzymes (Zhou and Chen, 2001; Arslan et al., 2011). To understand the potential measurement errors for glucose and lactate due to changing buffer pH during experiments, we also measured the effect of pH change on lactate and glucose sensors responses and added pH as a calibration variable.

2.5.2. Calibration for pH sensor

Solutions of different pH values were made by diluting sodium hydroxide (NaOH) or hydrogen chloride (HCL) in 2 mM potassium chloride (KCl) using the concentration vs volume equation $C_1V_1 = C_2V_2$. The KCl solution was used for dilution to prepare solutions with different pH values with full ionic strength (Rubinson, 2017). Values for pH were validated using a commercial pH meter (Hanna instruments, Woonsocket RI, USA). The change in voltage corresponding to pH change were measured and recorded using an INA333-based instrumentation amplifier (Analog Devices, Norwood, MA) circuit.

2.6. Measurement setup

2.6.1. Oxygen, glucose, lactate and pH measurements

Medium temperature was maintained at 38.5 °C during measurement by placing the device on a stage warmer for a stereomicroscope. The respective activation voltages were applied during amperometric experiments for DO, glucose, and lactate.

The electrodes were rinsed using DI water and electrochemically pulse-cleaned for 1 min before and after each test. Sterilized DI water was used for pulse cleaning to avoid any toxic effect on cells from cleaning chemicals.

Two separate micro-chambers were used for measurements. One chamber was used for measuring oxygen and pH, and the other chamber was used for measuring glucose and lactate. To reliably measure the OCR, the embryo was put into the micro-chamber with the oxygen and pH sensors activated for a period of time sufficient for the OCR signal to reach a stable reading, followed by a reading of the pH value in the micro-chamber. The micro-chamber contained 250 μL of G-MOPS. Once stable readings were obtained, 2.5 μL of the G-MOPS medium each was extracted from the micro-chamber containing the embryo and moved into the second micro-chamber with the activated glucose and lactate sensors. Each extracted 2.5 μL of the G-MOPS medium covered the entire area of the glucose and lactate sensor, respectively. in the second micro-chamber. After measurements were completed, the extracted G-MOPS medium droplets were removed from the sensor sites, and the sensor sites were cleaned with DI water and dried for the next round of measurements. Due to the required enzymatic surface modifications for the glucose and lactate sensors and the proximity of the sensors inside the micro-chamber, the main reason for separating the micro-chambers is that enzymatic reactions on both the glucose and lactate sensors produce H_2O_2 which is electrochemically detected by the sensor. The proximity of the sensors within the micro-chamber could create interference due to the diffusion of H_2O_2 between sensor sites. Although we do not know if any interference could have impacted the accuracy of the glucose and lactate measurements, we were cautious to avoid the possibility of such interference during the experiments. Further studies of interference and its preliminary findings are discussed later in this paper.

Equine embryos from four different stages were used for these experiments. They are labeled from Groups 1–4 for small or early blastocysts (SB/EB), blastocysts (B), expanded blastocysts (XB), and non-viable (dead) embryos, respectively (see S.4 in Supplementary material). OCR and pH were measured in two cycles. In each cycle, oxygen was measured for 10–12 min, and pH was measured for 2 min. Two droplets of 2.5 μL of G-MOPS each were then removed and placed on top of the glucose and lactate sensors, respectively, for 2 min each to obtain glucose and lactate readings. The cycles were repeated after adding oligomycin (1 μM) as an ATP synthase inhibitor and three FCCP titrations (1 μM) as a way to reveal the maximal cellular respiratory capacity.

The OCR, GCR, and LPR were calculated based on a model in our previously published papers (Obeidat et al., 2018a, 2018b) and included in S.8 in the Supplementary material.

The pH change was measured by converting the change in voltage during cell respiration in a defined buffer volume to pH level change using the calibration curve and the following equation:

$$\Delta pH = \frac{\Delta V}{\text{sensitivity}\left(\frac{mV}{pH}\right)} \quad (1)$$

where ΔV is the measured change in voltage, and the sensitivity is the slope of pH sensor calibration curve.

2.7. Sensor interference tests

Interference between the glucose and the lactate sensors may exist if the glucose and lactate working electrodes are close to each other. The enzymatically generated H_2O_2 at one sensor site (e.g. the lactate sensor) can be diffused to the nearby glucose sensor over time that also relies on H_2O_2 production to generate redox current. To reduce the possibility of interference, one can increase the separation distance between the working electrodes. However, this will make the micro-chamber bigger, thus, reducing sensitivity. Furthermore, the degree of interference also depends on the intrinsic quantities of associated target analytes in the buffer. We have previously illustrated the effect of interference between glucose and lactate sensors within a single micro-chamber (Obeidat et al., 2018b) where the detectable amount of diffused H_2O_2 took about 40 min to reach the affected sensor.

To further understand inter-sensor interference and their relationships with sensor distance and measured target analyte concentration in a given buffer, a multi-sensor configuration was used with smaller sensor distances for interference experiments (Fig. 1**B**). This configuration is also shown in S.17 in Supplementary material. The interference tests used three of the four corner sensors shown in Fig. 1**B**. One sensor was the initiating sensor, and the other two sensors were receiving sensors with distances of 3.2 and 4.6 mm to the initiating sensor, respectively. The initiating sensor produces H_2O_2 from its enzyme layer from one of the analytes (glucose or lactate); the receiving sensors are turned on to electrochemically detect traces of H_2O_2 diffused from the initiating sensors under four different concentrations of glucose and lactate (0.1 mM, 0.5 mM, 1 mM and 2 mM). These participating sensors were monitored simultaneously for 2 h for each concentration.

3. Results and discussion

3.1. Sensors calibration and stability

3.1.1. pH sensor calibration

Fig. 2**A** shows the pH sensor calibration results, the sensor has a wide dynamic range from pH 1 to pH 14, a good linearity of 0.99 and a sensitivity of −54.74 mV/pH that is close to what was reported in a

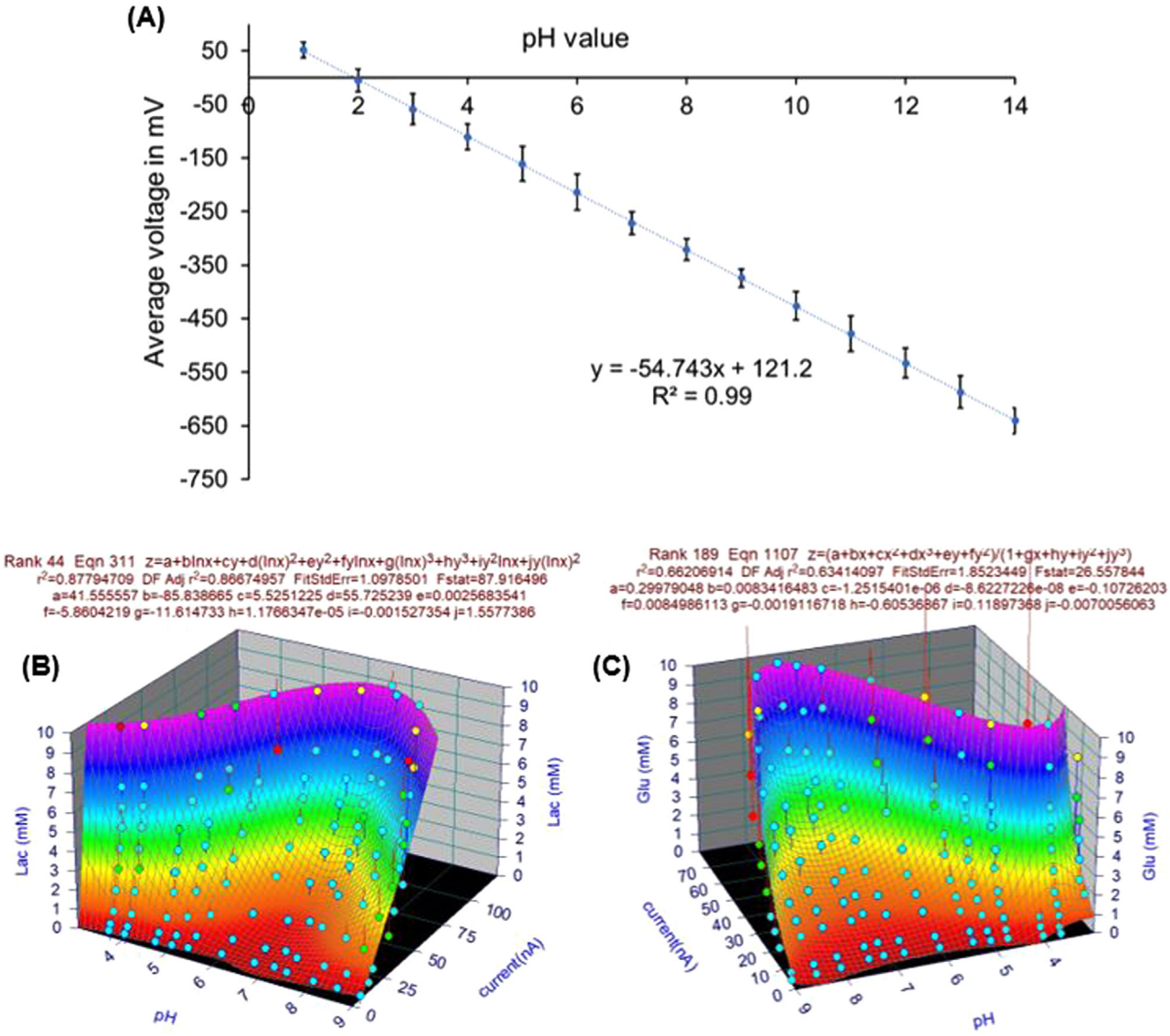

Fig. 2. (A) pH sensor calibration curve (Error bars in each curve are standard deviations (SD) between 6 data points). **(B)** Lactate sensor 3D calibration curve. **(C)** Glucose sensor 3D calibration curve.

previous study (Liao et al., 1998). A voltage difference of 5.5 mV is equivalent to a pH-difference of about 0.1 pH. The measured pH level of the baseline which represents GMOP before injecting the cell is 7.47 ± 0.07 (or −280.1 ± 1.4 mV in measured voltage). ECAR was measured by taking the change in pH level vs the baseline after adding the cell.

3.1.2. Oxygen, glucose and lactate sensors calibration results

Similar to those in our previous paper (Obeidat et al., 2018b), the results of oxygen, glucose, and lactate sensor calibration with a fixed pH value are included in S.9 in Supplementary material. However, as discussed in Section 2.5.1, calibrations for glucose and lactate sensors should also include the impact of changing pH during the experiments. The new calibration surfaces with pH as one of the variables for glucose and lactate are presented in Fig. 2**B and C**. Our results are consistent with previously published results (Zhou and Chen, 2001; Arslan et al., 2011). The changing pH makes glucose and lactate readings, based on the calibration curve with a fixed pH value, deviate from their true readings.

3.1.3. Stability of the sensors

Although from the stability point of view, the use of Ag/AgCl as a RE is better. However, gold (Au) was used as pseudo RE. The use of Au as reference electrode material for our multi-sensor platform is mainly due to 1) manufacturing compatibility and simplicity of the sensor substrate. The electrode substrate (glass substrate) of our multi-sensor system is set up to be disposable. Therefore, keeping the overall manufacturing costs down using the same material for all electrodes in the system is one of the main goals. 2) The advantage of stability using Ag/AgCl reference electrode is greatly reduced due to the fact that our multi-sensor electrode substrate is intended to be one-time use only. 3) The potential shift of pseudo-reference electrode such as Au electrode is insignificant in the short time period of its use. The potential shift over longer period of time due to surface polarization does not impact our system.

3.2. Characterization of equine embryo energy metabolism

3.2.1. Evaluation of equine embryo metabolism

The patterns of OCR, GCR, LPR and ECAR were analyzed by one-way analysis of variance (ANOVA) among different stages. Differences

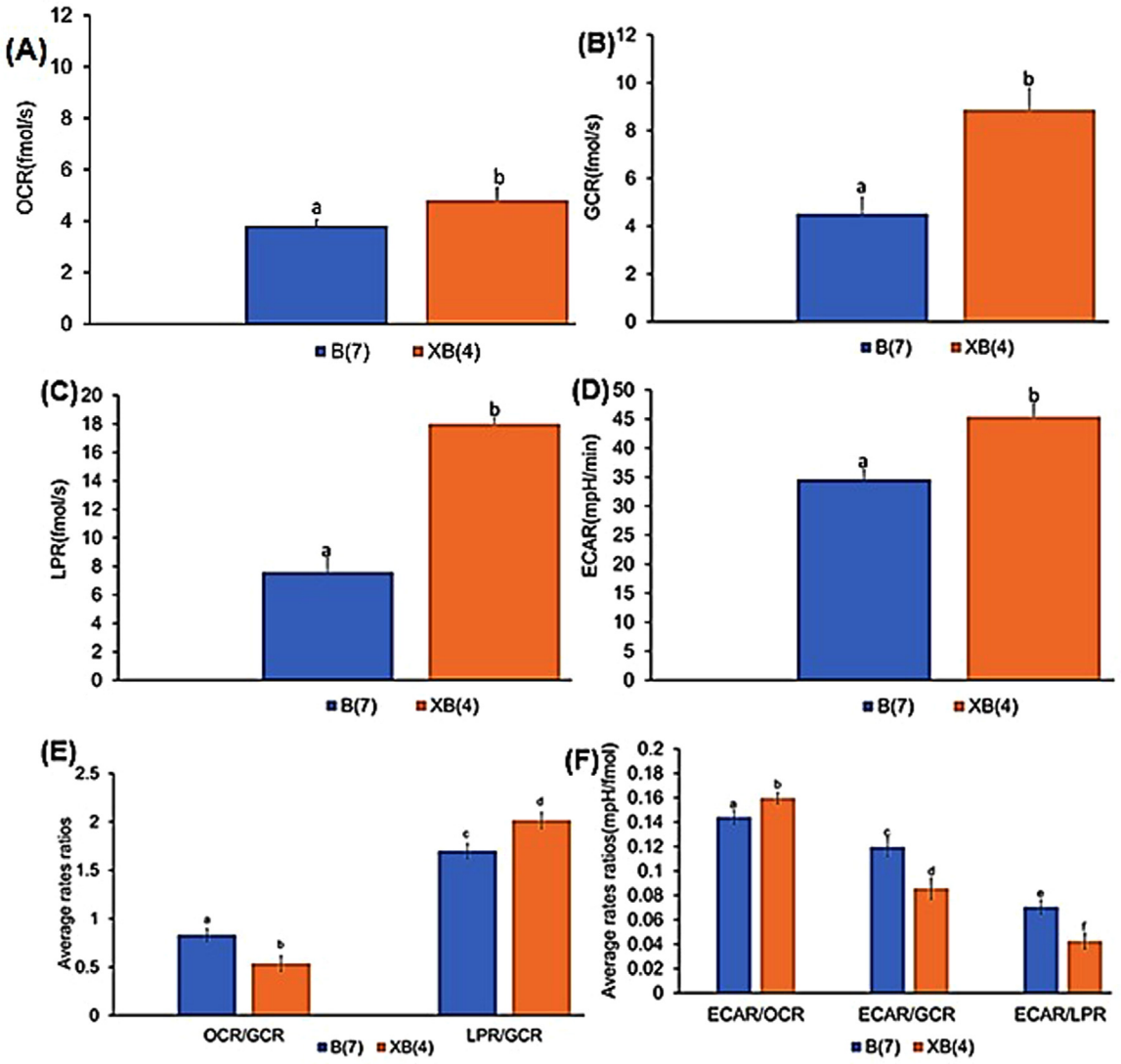

Fig. 3. Rates for B and XB equine embryos: **(A)** basal OCR **(B)** basal GCR **(C)** basal LPR **(D)** basal ECAR **(E)** basal OCR/GCR and LPR/GCR **(F)** basal ECAR/OCR, ECAR/GCR and ECAR/LPR. (mean ± standard of error (SE), $P \leq 0.05$).

between individual means were examined using Tukey HSD (pairwise comparison among stages). As metabolic end points were similar for embryos in early or small blastocyst and blastocyst stages, the stages were combined into blastocyst (B) for comparison with expanded blastocysts (XB). Nonviable embryos showed minimum basal respiration and a minimum response to oligomycin and FCCP when compared to viable embryos (see S.15 and Tables S.2 to S.4 in Supplementary material).

All parameters of basal metabolic flux (OCR, GCR, LPR, and ECAR) increased ($P \leq 0.05$) from B and XB stages in viable equine embryos (Fig. 3**A-D**); see Tables S.2 to S.4 in Section S.16 in Supplementary material for pairwise comparisons). The observed increases in basal OCR, GCR, LPR, from B to XB are consistent with our previous study on bovine embryos (Obeidat et al., 2018b) and previous studies (Guerif et al., 2013), and generally reflect the increase in embryo energy and nutrient demands as cell numbers increase (Hardy et al., 1989). The observed increase of ECAR from B to XB stage suggests a greater reliance on glycolysis to meet energy demands during blastocyst expansion, consistent with the observed increase in LPR. This is further supported by a decline in the OCR/GCR ratio, indicating a lesser contribution of OXPHOS to total glucose utilization, and higher LPR/GCR ratio, suggesting a greater utilization of glucose for lactate production, from B to XB (Fig. 3**E**), consistent with our previous findings (Obeidat et al., 2018b). Interestingly, integrating ECAR into these metabolite flux analyses revealed insights that highlight the greater complexity of metabolic substrate utilization in developing embryos (Fig. 3**F**). As expected, the ECAR/OCR increased from B to XB, which is viewed as a greater contribution of glycolysis relative to OXPHOS. However, both ECAR/GCR and ECAR/LPR declined from B to XB, indicating a greater proportion of glucose consumed by expanded blastocysts is not contributing to ECAR. Interpretation of this result requires a more comprehensive view of nutrient metabolism and the potential courses of OCR and ECAR in developing embryos, which is summarized in Fig. 4.

Importantly, a developing embryo uses glucose both for ATP production and biosynthetic processes that are essential for cell growth and proliferation (Krisher and Prather, 2012). These pathways (in particular, the pentose phosphate and one-carbon metabolism pathways) result in much less CO_2 production or and net H+ released from glucose consumed because more of the carbons of glucose (and other nutrients) stay inside the cell to build cellular components such as DNA, proteins, and lipids, as well as mediate epigenetic programming (methylation) of developing genes (Kalhan, 2016; Wales and Du, 1993). Therefore, the lower ECAR relative to glucose utilization in expanding blastocysts likely reflects an increasing proportion of glucose uptake contributing to biosynthetic processes rather than glycolytic ATP production. Moreover, shifts in the uptake and utilization of other

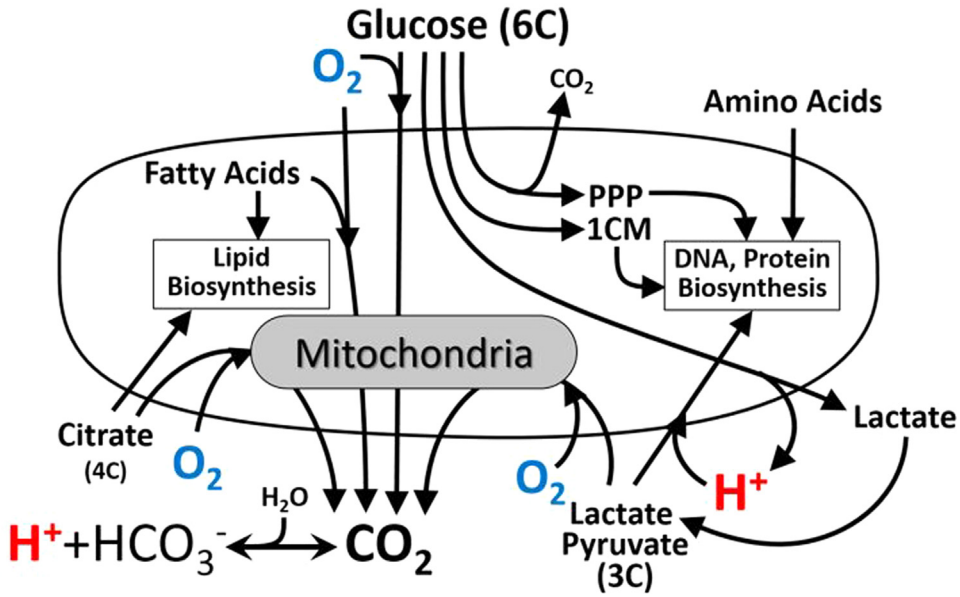

Fig. 4. Sources of OCR and ECAR and metabolite flux in developing embryos. Oxygen (O_2) is consumed by respiring mitochondria in cells to support oxidative metabolism of multiple substrates. Hydrogen ions (H+) are exported from cells with lactate but can also be generated from CO_2 in the aqueous G-MOPS buffer or co-transported into cells along with pyruvate or lactate. The six carbons of glucose can be released as CO_2 during oxidative metabolism, as two lactate molecules following glycolysis, or utilized in the biosynthetic pentose phosphate pathway (PPP) and one-carbon metabolism (1CM) pathway.

metabolic substrates (e.g., pyruvate and fatty acids) can decrease the net cellular release of H+ and alter the stoichiometry of OCR and CO_2 production, further complicating interpretation of changes in ECAR and OCR. Similar metabolic shifts occur in proliferating cancer cells (Rosenzweig et al., 2018; Ducker and Rabinowitz, 2017), and are being increasingly recognized as an important consideration in the study of cellular glucose utilization and bioenergetics in this context (DeBerardinis and Chandel, 2016). Therefore, integrating simultaneous OCR and ECAR measurements with real-time metabolite flux analyses can significantly improve the interpretive value of isolated measurements performed in these complex metabolic systems. The multi-sensor approach described herein provides a miniaturized platform for performing these integrative analyses in very small primary samples, which could be complimented by additional metabolite sensors or stable isotope-tracer technologies to further elucidate metabolic aspects of cellular development and proliferation in health and disease.

3.2.2. *Effect of oligomycin and FCCP titration on embryo metabolism*

Fig. 5**A-D** illustrate the combined averages of OCR, GCR, LPR and ECAR in embryos at all developmental stages under basal conditions followed by the subsequent titration of oligomycin and FCCP (complete data from all developmental stages are presented in S.15 of Supplementary material). As expected, oligomycin stopped OCR and forced embryos to rely more heavily on glucose metabolism indicated by higher GCR, LPR and ECAR. FCCP was then carefully titrated in 1 μM steps to pinpoint the maximal "non-coupled" rate of embryo OCR (at ~2 μM), after which an inhibitory effect becomes evident (see S.15 in Supplementary material). This acceleration of uncoupled OCR by FCCP further increased GCR, and to a lesser extent LPR, consistent with a re-activation of glucose oxidation by mitochondria, but continued reliance on glycolytic ATP production due to inhibition of mitochondrial ATP production. However, this uncoupling of mitochondrial respiration with FCCP strongly decreased ECAR, suggesting a significant shift in embryo redox state under these conditions. FCCP collapses the mitochondrial membrane potential, leading to acidification of the mitochondrial matrix until it equilibrates with the cell H+ content. This creates a redox imbalance in the cytosol that favors cellular retention of H+ to maintain reducing power, perhaps leading to lower net release of H+ observed as lower ECAR. Mitochondrial substrate handling and oxidative potential may also become progressively disrupted, perhaps favoring a lower net release of CO_2 that contributes to ECAR resulting from carbonic acid buffering in the media (Fig. 4). The precise mechanisms at play under these experimental conditions require more sophisticated methods to elucidate fully, but the results of these studies highlight the distinctions between ECAR and glucose utilization that could be leveraged using a multi-sensor approach to study the links between cell metabolism and redox function.

Calculation of metabolite flux ratios (Fig. 5**E and F**) further emphasizes this point. Inhibition of mitochondrial ATP production with oligomycin significantly increased the embryo LPR/GCR, ECAR/GCR and ECAR/LPR ratios, consistent with the expected "switch" from glucose-supported OXPHOS to anaerobic glycolysis (lactate fermentation) in order to maintain cellular ATP production. However, maximizing uncoupled mitochondrial respiration and substrate oxidation rates with FCCP decreased ECAR relative to all other metabolite flux rates (Fig. 5**F**), as well as LPR/GCR and OCR/GCR (Fig. 5**E**), reflecting marked shifts in cellular substrate and H+ handling that dissociate elevated rates of glucose and lactate flux from ECAR. The decrease in OCR/GCR, in particular, suggests a greater utilization of non-glucose substrates to support the elevated rates of OCR under these conditions (Fig. 4), highlighting the complexity of this metabolic system and value of simultaneous monitoring of multiple metabolites for more comprehensive studies of embryo function during development.

3.2.3. *Effect of changing pH on glucose and lactate measurements*

The obtained glucose and lactate measurements based on the calibration curve obtained assuming a fixed pH value have errors due to our ignoring pH changes during cell basal respiration and glycolysis. Using the calibration surfaces in Fig. 2**B and C**, we examined the amount of errors associated with the glucose and lactate measurements presented in Figs. 3 and 5. Table S.5 in S.19 in Supplementary material. The maximum errors for each measurement phase are shown to range from 6.2% to 9.7%. The models in Fig. 2**B and C** provide a general assessment for glucose and lactate measurement accuracy due to changing pH. The model fitting errors also contribute to the overall error. Better models using a region-based multi-dimensional data interpretation to minimize fitting errors are under development for measurement data correction in the future.

3.3. *Sensor interference between glucose and lactate sensors*

Cross-diffusion of H_2O_2 generated at the anzyme at the glucose and lactate sensors is a potential source of interference if both sensors reside within the same micro-chamber (Fig. 1**B**). The extent of interference

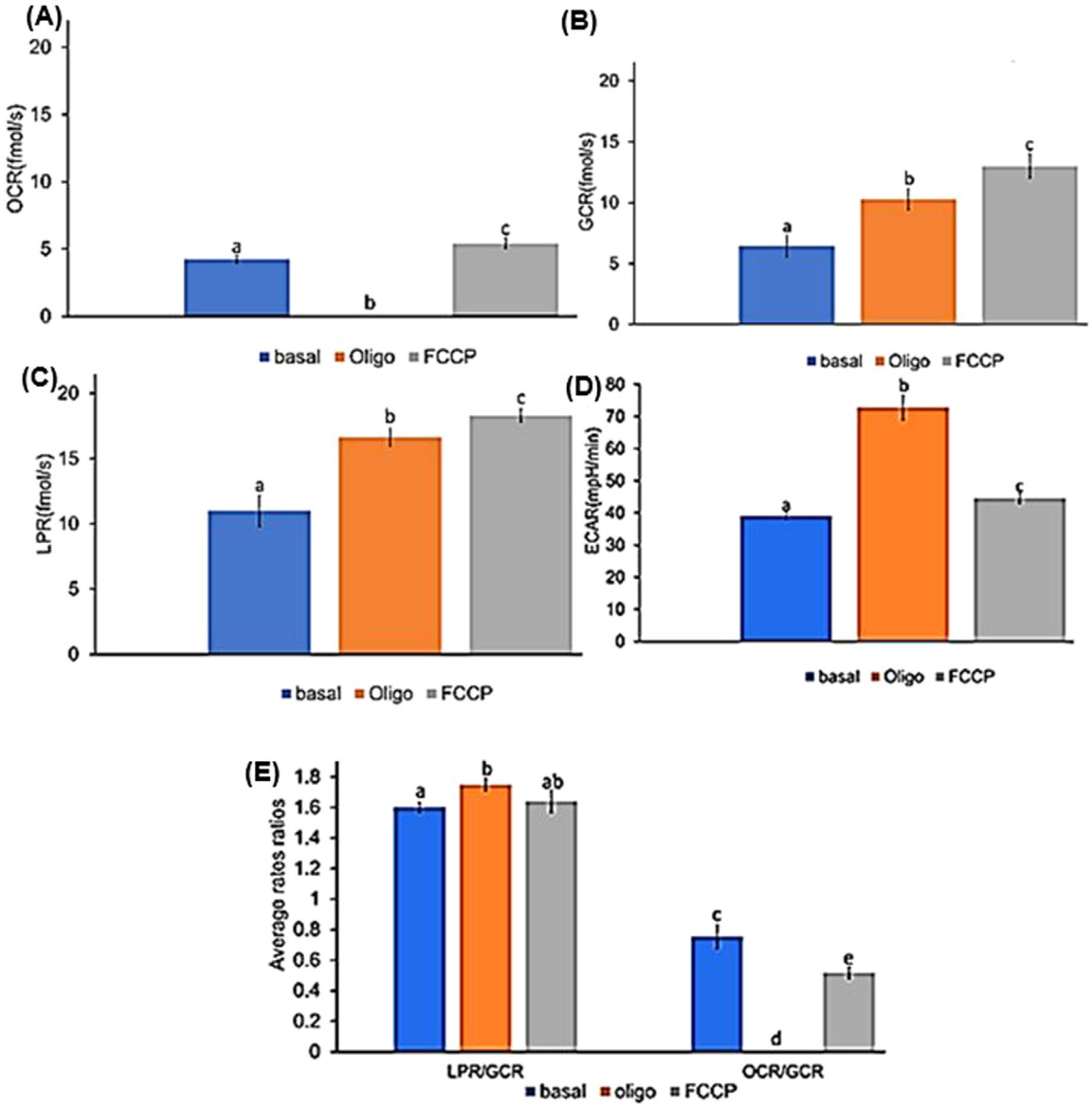

Fig. 5. Rates for all equine embryos under conditions of (basal, oligomycin(oligo), and FCCP): **(A)** OCR **(B)** GCR **C)** LPR **(D)** ECAR **(E)** Flux ratios (LPR/GCR and OCR/GCR). (mean ± SE, n = 11, P ≤ 0.05).

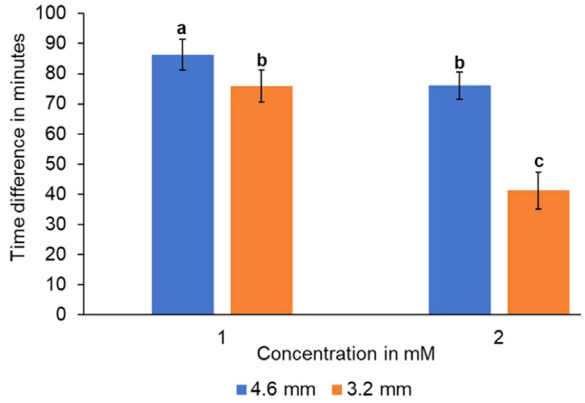

Fig. 6. Amount of time (min) vs concentration (mM) at different distances. (mean ± SD, n = 8, P ≤ 0.05).

could be influenced by substrate concentration at the initiating sensor and the distance between the two sensors. At concentrations of 0.1 mM and 0.5 mM of the initiating analytes (glucose or lactate), there was no detectable H_2O_2 diffusion from initiating to receiving sensors at either distance examined (see S.19 in Supplementary material). Interference was detectable when the initiating analyte concentrations were increased to 1 mM and 2 mM, with cross-diffusion times ranging from 40 to 85 min (Fig. 6). These studies indicate that substrate concentration and sensor spacing are potentially important considerations in multi-sensor designs. Interference can be minimized by running shorter experiments or isolated sensors in satellite sampling chambers as was done in the studies presented in Figs. 3 and 5.

4. Conclusions and future work

This paper presents a multi-sensor platform for real-time analysis of glucose metabolism, ECAR, and mitochondrial respiration for small biological samples such as single equine embryos. The collection of multiple metabolites allows more meaningful analysis of cell metabolism than previously possible. For example, the availability of OCR,

GCR, and LPR from the same biological sample during the same time period allows one to determine composite measurements such as metabolite flux ratios (OCR vs. GCR, and LPR vs. GCR) to provide better insight into embryo metabolism. Our results using the metabolite flux ratios further highlight the "switch" from glucose-supported OXPHOS to anaerobic glycolysis (lactate fermentation) in order to maintain cellular ATP production when inhibition of mitochondrial ATP production occurs. We have also demonstrated the ability to integrate ECAR into the multi-sensor platform for the first time under multiple physiological and experimental conditions. Contrary to common practice of using ECAR as a predominant marker for glycolysis, our results highlight that integrating simultaneous OCR, GCR, LPR, and ECAR measurements with real-time metabolite flux analyses can significantly improve the interpretive value of isolated measurements performed in these complex metabolic systems. This was illustrated by our detailed analysis of the complex relationship of ECAR/GCR and ECAR/LPR relative to cell's metabolic stages. We also presented the sensor interference results between enzymatic sensors in close proximity. These preliminary results will guide optimization of future sensor design to minimize interference. Further enhancements of the platform include addressing challenges associated with handling and positioning of small biological samples, such as embryos, for analyses through addition of microscopy and microfluidic channels. Future applications of the platform include real-time metabolic analysis of single cells or small multicellular samples obtained from heterogeneous tissues such as tumors or granulomas relevant to cancer and infectious disease.

CRediT authorship contribution statement

Yusra M. Obeidat: Methodology, Investigation, Writing - review & editing. **Ming-Hao Cheng:** Investigation, Methodology. **Giovana Catandi:** Methodology, Investigation. **Elaine Carnevale:** Conceptualization, Methodology, Writing - review & editing. **Adam J. Chicco:** Conceptualization, Methodology, Writing - review & editing. **Thomas W. Chen:** Supervision, Conceptualization, Methodology, Writing - review & editing.

Acknowledgements

The results presented in this paper are based upon collaborative work supported by a National Science Foundation, USA, NRT Grant No. 1450032 and by MRI program under Grant No. 1727044. Additional funding was also provided by Colorado's Advanced Industries program through an OEDIT grant from the State of Colorado, USA. The authors would also like to thank August DeMann and Stuart Field for their support in metal evaporation and JoAnne Stokes from the Equine Research Lab (ERL) at Colorado State University for her assistance in some experiments.

Declaration of interest statement

The authors declare that they have no known competing financial interests or personal relationships that could have appeared to influence the work reported in this paper.

Appendix A. Supporting information

Supplementary data associated with this article can be found in the online version at doi:10.1016/j.bios.2019.02.069.

References

Arslan, F., Ustabaş, S., Arslan, H., 2011. An amperometric biosensor for glucose determination prepared from glucose oxidase immobilized in polyaniline-polyvinylsulfonate film. Sensors (Basel Switz.) 11 (8), 8152–8163. https://doi.org/10.3390/s110808152.

Bavli, D., Prill, S., Ezra, E., Levy, G., Cohen, M., Vinken, M., Vanfleteren, J., Jaeger, M., Nahmias, Y., 2016. Real-time monitoring of metabolic function in liver-on-chip microdevices tracks the dynamics of mitochondrial dysfunction. Proc. Natl. Acad. Sci. USA 113, E2231–E2240. https://doi.org/10.1073/pnas.1522556113.

Bennett, B., Jetton, T., Ying, G., Magnuson, M., Piston, D., 1996. Quantitative subcellular imaging of glucose metabolism within intact pancreatic islets. J. Biol. Chem. 271 (7), 3647–3651. https://doi.org/10.1063/1.4955155.

Butler, M., 2005. Animal cell cultures: recent achievements and perspectives in the production of biopharmaceuticals. Appl. Microbiol. Biotechnol. 68, 283–291. https://doi.org/10.1007/s00253-005-1980-8.

Ducker, G.S., Rabinowitz, J.D., 2017. One-carbon metabolism in health and disease. Cell Metab. 25, 27–42. https://doi.org/10.1016/j.cmet.2016.08.009.

DeBerardinis, R.J., Chandel, N.S., 2016. Fundamentals of cancer metabolism. Sci. Adv. 2, e1600200. https://doi.org/10.1126/sciadv.1600200.

Eklund, S., Taylor, D., Kozlov, E., Prokop, A., Cliffel, D., 2004. A microphysiometer for simultaneous measurement of changes in extracellular glucose, lactate, oxygen, and acidification rate. Anal. Chem. 76 (3), 519–527. https://doi.org/10.1021/ac034641z.

Feuerstein, D., Manning, A., Hashemi, P., Bhatia, R., Fabricius, M., Tolias, C., Pahl, C., Ervine, M., Strong, A.J., Boutelle, M.G., 2010. J. Cereb. Blood Flow. Metab. 30, 1343–1355 (PubMed: 20145653).

Guerif, F., McKeegan, P., Leese, H.J., Sturmey, R.J., 2013. A simple approach for consumption and release (CORE) analysis of metabolic activity in single mammalian embryos. PLoS One 8, e67834. https://doi.org/10.1371/journal.pone.0067834.

Hardy, K., Hooper, M.A., Handyside, A.H., Rutherford, A.J., Winston, R.M., Leese, H.J., 1989. Non-invasive measurement of glucose and pyruvate uptake by individual human oocytes and preimplantation embryos. Hum. Reprod. 4, 188–191 PMID: 2918073.

Kalhan, S.C., 2016. One carbon metabolism in pregnancy: impact on maternal, fetal and neonatal health. Mol. Cell. Endocrinol. 435, 48–60. https://doi.org/10.1016/j.mce.2016.06.006.

Krisher, R.L., Prather, R.S., 2012. A role for the Warburg effect in preimplantation embryo development: metabolic modification to support rapid cell proliferation. Mol. Reprod. Dev. 79, 311–320. https://doi.org/10.1002/mrd.22037.

Lambert, A., Brand, M., 2007. Research on mitochondria and aging. Aging Cell 6, 417–420. https://doi.org/10.1111/j.1474-9726.2007. 00316.x.

Liao, H.-K., Chou, J.-C., Chung, W.-Y., Sun, T.-P., Hsiung, S.-K., 1998. Study of amorphous tin oxide thin films for ISFET applications. Sens. Actuators B 50, 104–109. https://doi.org/10.1016/S0925-4005(98)00162-2.

McConnell, H., Owicki, J., Parce, J., Miller, D., Baxter, G., Wada, H., Pitchford, S., 1992. The cytosensor microphysiometer: biological applications of silicon technology. Science 257, 1906–1912. https://doi.org/10.1126/science.1329199.

Mookerjee, S., Brand, M., 2015. Measurement and analysis of extracellular acid production to determine glycolytic rate. J. Vis. Exp. 106, e53464. https://doi.org/10.3791/53464.

Mousavi, S., De Ferrari, F., Zhang, Y., Nabavinia, M., Binth Mohammad, N., Ryan, J., Pourmand, A., Laukaitis, E., Banan Sadeghian, R., Nadhman, A., Shin, S., Nezhad, A., Khademhosseini, A., Dokmeci, M., 2016. A microfluidic optical platform for real-time monitoring of pH and oxygen in microfluidic bioreactors and organ-on-chip devices. Biomicrofluidics 10, 044111. https://doi.org/10.1063/1.4955155.

Nicholls, D., Johnson-Cadwell, L., Vesce, S., Jekabsons, M., Yadava, N., 2007. Bioenergetics of mitochondria in cultured neurons and their role in glutamate excitotoxicity. J. Neurosci. Res. 85, 3206–3212. https://doi.org/10.1002/jnr.21290.

Obeidat, Y., Chen, T., 2016. Characterization of an O_2 sensor using microelectrodes. IEEE sensors. IEEE Sensors Orlando FL. https://doi.org/10.1109/ICSENS.2016.7808460. (Oct. 30 – Nov. 2).

Obeidat, Y., Evans, A., Tedjo, W., Chicco, A., Carnevale, E., Chen, T., 2018a. Monitoring oocyte/embryo respiration using electrochemical-based oxygen sensors. Sens. Actuators: B. Chem. https://doi.org/10.1016/j.snb.2018.07.157.

Obeidat, Y., Catandi, G., Carnevale, E., Chicco, A., DeMann, A., Field, S., Chen, T., 2018b. A multi-sensor system for measuring bovine embryo metabolism. Biosens. Bioelectron. https://doi.org/10.1016/j.bios.2018.09.071.

Owicki, J., Parce, J., 1992. Biosensors based on the energy metabolism of living cells: the physical chemistry and cell biology of extracellular acidification. Biosens. Bioelectron. 7, 255–272. https://doi.org/10.1016/0956-5663(92)87004-9.

Pemberton, R., Cox, T., Tuffin, R., Drago, G.A., Griffiths, J., Pittson, R., Johnson, G., Xu, J., Sage, I., Davies, R., Jackson, S., Kenna, G., Luxton, R., Hart, J., 2014. Fabrication and evaluation of a micro(bio)sensor array chip for multiple parallel measurements of important cell biomarkers. Sensors (Basel Switz.) 14 (11), 20519–20532. https://doi.org/10.3390/s141120519.

Pemberton, R., Pittson, R., Biddle, N., Hart, J., 2009. Fabrication of microband glucose biosensors using a screen-printing water-based carbon ink and their application in serum analysis. Biosens. Bioelectron. 24, 1246–1252. https://doi.org/10.1016/j.bios.2008.07.035.

Pilatus, U., Aboagye, E., Artemov, D., Mori, N., Ackerstaff, E., Bhujwalla, Z., 2001. Real-time measurements of cellular oxygen consumption, pH, and energy metabolism using nuclear magnetic resonance spectroscopy. Magn. Reson. Med. 45 (5), 749–755. https://doi.org/10.1002/mrm.1102.

Rawson, F., Purcell, W., Xu, J., Pemberton, R., Fielden, P., Biddle, N., Hart, J., 2009. A microband lactate biosensor fabricated using a water-based screen-printed carbon ink. Talanta 77, 1149–1154.

Rubinson, K., 2017. Practical corrections for p(H, D) measurements in mixed H_2O/D_2O biological buffers. Anal. Methods 9 (18), 2744–2750. https://doi.org/10.1039/C7AY00669A.

Rosenzweig, A., Blenis, J., Gomes, A.P., 2018. Beyond the Warburg effect: how do cancer cells regulate one-carbon metabolism? Front. Cell Dev. Biol. 6, 90. https://doi.org/

10.3389/fcell.2018.00090.
Scott, R., Zhang, M., Seli, E., 2018. Metabolism of the oocyte and the preimplantation embryo: implications for assisted reproduction. Curr. Opin. Obstet. Gynecol. 30, 163–170. https://doi.org/10.1097/GCO.0000000000000455.
Sridharan, V., Guichard, J., Bailey, R., Kasiganesan, H., Beeson, C., Wright, G., 2007. The prolyl hydroxylase oxygen-sensing pathway is cytoprotective and allows maintenance of mitochondrial membrane potential during metabolic inhibition. Am. J. Physiol. Cell Physiol. 292, C719–C728. https://doi.org/10.1152/ajpcell.00100.2006.
TeSlaa, T., Teitell, M., 2014. Techniques to monitor glycolysis. Methods Enzymol. 542, 91–114. https://doi.org/10.1016/B978-0-12-416618-9.00005-4.
Vasdekis, A.E., Stephanopoulos, G., 2015. Review of methods to probe single cell metabolism and bioenergetics. Metab. Eng. 27, 115–135. https://doi.org/10.1016/j.ymben.2014.09.007.
Wales, R.G., Du, Z.F., 1993. Contribution of the pentose phosphate pathway to glucose utilization by preimplantation sheep embryos. Reprod. Fertil. Dev. 5329–5340. https://doi.org/10.1071/RD9930329.
Wang, X., Wolfbeis, O., 2014. Optical methods for sensing and imaging oxygen: materials, spectroscopies andi applications. Chem. Soc. Rev. 43, 3666–3761. https://doi.org/10.1039/c4cs00039k.
Wang, Y., Noël, J., Velmurugan, J., Nogala, W., Mirkin, M., Lu, C., Guille Collignon, M., Lemaître, F., Amatore, C., 2012. Nanoelectrodes for determination of reactive oxygen and nitrogen species inside murine macrophages. Proc. Natl. Acad. Sci. USA 2012 (109), 11534–11539. https://doi.org/10.1073/pnas.1201552109.
Watanabe, M., Houten, S., Mataki, C., Christoffolete, M., Kim, B., Sato, H., Messaddeq, N., Harney, J., Ezaki, O., Kodama, T., Schoonjans, K., Bianco, A., Auwerx, J., 2006. Bile acids induce energy expenditure by promoting intracellular thyroid hormone activation. Nature 439, 484–489. https://doi.org/10.1038/nature04330.
Wu, S., Wu, S., Yi, Z., Zeng, F., Wu, W., Qiao, Y., Zhao, X., Cheng, X., Tian, Y., 2018. Hydrogel-based fluorescent dual pH and oxygen sensors loaded in 96-well plates for high-throughput cell metabolism studies. Sensors 18, 564. https://doi.org/10.3390/s18020564.
Zhou, Q., Chen, X., 2001. Effects of temperature and pH on the catalytic activity of the immobilized β-galactosidase from Kluyveromyces lactis. Biochem. Eng. J. 9, 33–40.